A Pre-synchronization Strategy for Grid-forming Virtual Oscillator Controlled Inverters

Minghui Lu*, Soham Dutta*, Victor Purba†, Sairaj Dhople†, Brian Johnson*
*Department of Electrical and Computer Engineering, University of Washington, Seattle, WA 98195
†Department of Electrical and Computer Engineering, University of Minnesota, Minneapolis, MN 55455
Emails: {mhlu, sdutta, brianbj}@uw.edu, and {purba002, sdhople}@umn.edu

***Abstract*—Voltage controlled inverters in ac systems are susceptible to damage if the controller is not properly initialized before startup. Since currents are not controlled explicitly, the voltage reference of the controller must be closely aligned with the point of common coupling voltage to prevent large current transients when power delivery begins. In this paper, we are focused on a particular control strategy called virtual oscillator control and propose a *pre-synchronization* method that guarantees graceful addition of units into an existing ac system. The proposed method is generalized and can be used to add oscillator-controlled inverters to a stiff grid or an islanded microgrid with other inverters. An equivalent circuit model of the pre-synchronization control is derived along with its dynamical properties, design guidelines are given, and experimental results are shown for a $1.5\,$kW inverter.**

I. Introduction

Virtual oscillator control (VOC) is a grid-forming inverter control strategy wherein inverters are programmed to emulate the dynamics of weakly nonlinear limit-cycle oscillators such as dead-zone and Van der Pol oscillators [1]–[5]. Here, we use the term *grid-forming* to refer to inverters that not only have voltage control, but are also able to synchronize with each other and create multi-inverter ac systems via decentralized control [6]–[11]. (Perhaps the most classical and well-known controller of this type is droop control; VOC is a comparable recent technology.) Of key importance, interconnected inverters with VOC act as coupled oscillators that are able to achieve ac system-level objectives such as synchronization, power sharing, as well as voltage and frequency regulation, all without explicit communication [3], [12]. Analysis also shows that VOC subsumes the functionality of conventional droop control in steady state while providing enhanced dynamic speed due to its time-domain implementation [10], [13].

To incorporate real and reactive power setpoints, mitigate harmonics, and facilitate operation in both grid-connected and islanded systems, recent incarnations of VOC have been based on the so-called *Andronov-Hopf oscillator* (AHO) [14]–[17]. This oscillator provides the functionality of additional input signals that act as setpoints. This work provides a systematic startup strategy for VOC realized with Andronov-Hopf oscillator dynamics. The ideal startup routine would limit currents at startup and can be generalized to whether an inverter is interfaced to a stiff grid or an islanded system with other inverters. Such pre-synchronization routines have been previously devised in [18]–[21] for connecting voltage source inverters to an energized system running in either islanded or grid connected modes. In particular, [18] has proposed a pre-synchronization circuit for parallel voltage source inverters controlled using a virtual oscillator controller based on the Van der Pol oscillator. In [19], a pre-synchronization strategy is proposed to achieve seamless transfer from islanded to grid-connected mode for droop controlled inverters in a microgrid. To fill this gap for the case of parallel inverters controlled using the novel AHO-based virtual oscillator controller, we put forth a pre-synchronization controller (shaded blue in Fig. 1) that matches the phase, frequency, and amplitude of the internal voltage command with those of the measured point of common coupling voltage prior to startup. We point to [22] for a recent related effort in designing pre-synchronization routines for AHO-based controllers. In this work, staying aligned with the philosophy of VOC to promote circuit-based realizations of controllers, an equivalent-circuit model of the proposed pre-synchronization controller is also outlined. This facilitates the derivation of design guidelines.

The remainder of this paper is organized as follows: In Section II, we overview modeling preliminaries and the dynamic models for AHO control. Section III presents the analysis and implementation of the proposed pre-synchronization scheme. Equivalent circuit interpretation and parameter selection corresponding to the pre-synchronization scheme are provided in Section IV. Simulation and experimental validation follow in Section V. Finally, we conclude the paper in Section VI.

II. The Andronov-Hopf Oscillator Based Controller

In this section, we begin with an overview of the virtual oscillator controlled inverter configuration realized with the AHO. (See [14] for details.) Following this, we also provide the dynamical model description in a suitable reference frame.

This material is based upon work supported by the U.S. Department of Energy's Office of Energy Efficiency and Renewable Energy (EERE) under Solar Energy Technologies Office (SETO) Agreement Number EE0009025, the National Science Foundation through grant 1509277, and Washington Research Foundation.

978-1-7281-5826-6/20/$31.00 ©2020 IEEE

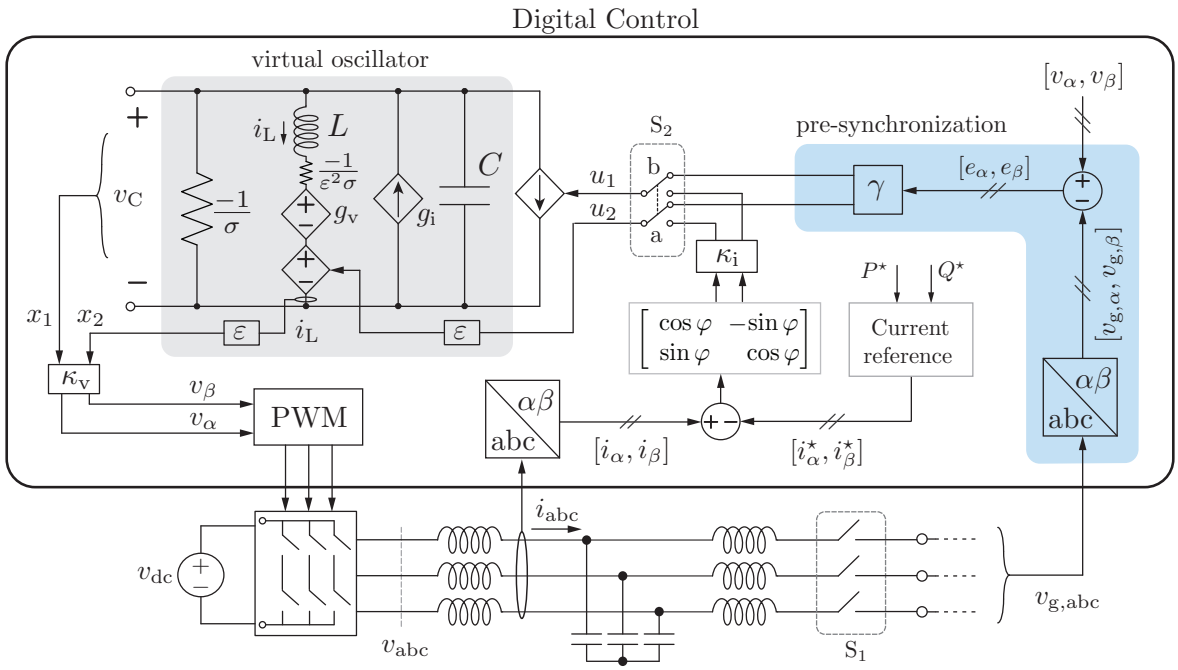

Fig. 1. A three-phase voltage source inverter with grid-compatible virtual oscillator controller (shaded gray) and pre-synchronization strategy (shaded blue).

A. Control Configuration

Consider a typical three-phase inverter, as shown in Fig. 1, where the physical hardware includes dc source $v_{\rm dc}$, a hex bridge, and an output LCL filter, followed by a relay switch S_1. Relevant control loops are digitally realized and the virtual oscillator (shaded gray) is composed of three main parts:

1) An LC tank with resonant frequency $\omega_{\rm nom} = 1/\sqrt{LC}$ and corresponding states $[x_1, x_2]^\top = [v_{\rm C}, \varepsilon i_{\rm L}]^\top$, where $\varepsilon = \sqrt{L/C}$ is the characteristic impedance. This LC tank serves the purpose of generating oscillating states.
2) Two resistors with negative conductances $-\sigma$ and $-\varepsilon^2\sigma$. These elements inject energy into the remainder of the circuit to sustain oscillations.
3) Nonlinear state-dependent voltage and current sources denoted by $g_{\rm v} = \varepsilon\alpha(v_{\rm C}^2 + \varepsilon^2 i_{\rm L}^2)\varepsilon i_{\rm L}$ and $g_{\rm i} = \alpha(v_{\rm C}^2 + \varepsilon^2 i_{\rm L}^2)v_{\rm C}$. These nonlinear elements facilitate obtaining a user-defined oscillation amplitude.

B. Dynamical Model Description

The differential equations of states $v_{\rm C}$ and $i_{\rm L}$ can be derived via fundamental circuit laws, and they are given by:

$$C\frac{{\rm d}v_{\rm C}}{{\rm d}t} = -i_{\rm L} - g_{\rm i} + \sigma v_{\rm C} - u_1, \tag{1}$$

$$L\frac{{\rm d}i_{\rm L}}{{\rm d}t} = v_{\rm C} - g_{\rm v} + \sigma\varepsilon(\varepsilon i_{\rm L}) - \varepsilon u_2, \tag{2}$$

where u_1 and u_2 are the input signals for the virtual oscillator, which are determined by the status of the virtual switch S_2, as shown in Fig. 1. When $\mathrm{S}_2 \to b$, the inverter will pre-synchronize to the bus voltage to avoid inrush current (the detailed analysis and parameter selection will be provided in subsequent sections); when $\mathrm{S}_2 \to a$, the inverter operates in a normal power regulating mode. The dynamics of inverter output voltages v_α, v_β are obtained by scaling the orthogonal states $v_{\rm C}$ and $\varepsilon i_{\rm L}$ by $\kappa_{\rm v}$ [14]:

$$\begin{bmatrix}\dot v_\alpha\\ \dot v_\beta\end{bmatrix} = \begin{bmatrix}\frac{\xi}{\kappa_{\rm v}^2}\left(2V_{\rm nom}^2 - \|v_{\alpha\beta}\|^2\right) & -\omega_{\rm nom}\\ \omega_{\rm nom} & \frac{\xi}{\kappa_{\rm v}^2}\left(2V_{\rm nom}^2 - \|v_{\alpha\beta}\|^2\right)\end{bmatrix}\begin{bmatrix}v_\alpha\\ v_\beta\end{bmatrix} - \underbrace{\frac{\kappa_{\rm v}}{C}\kappa_{\rm i}\begin{bmatrix}\cos\varphi & -\sin\varphi\\ \sin\varphi & \cos\varphi\end{bmatrix}\begin{bmatrix}i_\alpha - i_\alpha^\star\\ i_\beta - i_\beta^\star\end{bmatrix}}_{u}, \tag{3}$$

where $\|v_{\alpha\beta}\| := (v_\alpha^2 + v_\beta^2)^{1/2}$ is the Euclidean norm of $[v_\alpha, v_\beta]^\top$, $V_{\rm nom}$ is the nominal inverter voltage RMS amplitude, and ξ is a gain which influences convergence speed. With voltage setpoint $V_{\rm nom} > 0$, the state trajectories always spiral asymptotically towards a stable circular limit cycle with nominal RMS amplitude $V_{\rm nom}$ and rotation frequency $\omega_{\rm nom}$ regardless of initial states. Above, φ is a user-defined rotation angle that determines droop behavior in steady state, and the current references $i_\alpha^\star$ and $i_\beta^\star$ are calculated from the power references $P^\star$ and $Q^\star$ as follows:

$$\begin{bmatrix}i_\alpha^\star\\ i_\beta^\star\end{bmatrix} = \frac{2}{3\|v_{\alpha\beta}\|^2}\begin{bmatrix}v_\alpha & v_\beta\\ v_\beta & -v_\alpha\end{bmatrix}\begin{bmatrix}P^\star\\ Q^\star\end{bmatrix}. \tag{4}$$

III. Proposed Pre-synchronization Strategy

To guarantees smooth addition of inverter units, in this section, we formulate a systematic pre-synchronization control strategy for virtual oscillator controlled inverters.

A. Practical Implementation

We show the specific pre-synchronization implementation in Fig. 1, where switch S_2 status determines the inverter operational mode. Here, $(\mathrm{S}_2 \to \mathrm{a})$ corresponds to normal operation with nonzero power delivery, and $(\mathrm{S}_2 \to \mathrm{b})$ implies operation in pre-synchronization mode with zero power delivery. The input vector $[u_1, u_2]^\top$ takes on different values that depend on the status of S_2. In normal condition, the input vector is given by the term denoted as u in (3). When in pre-sychronization mode (i.e., $(\mathrm{S}_2 \to \mathrm{b})$), the input vector in (3) is proportional to the error $e_{\alpha\beta}$ between $v_{\alpha\beta}$ and ac bus voltage $v_{\mathrm{g},\alpha\beta}$ as follows:

$$\begin{bmatrix} u_1 \\ u_2 \end{bmatrix} = \gamma \begin{bmatrix} e_\alpha \\ e_\beta \end{bmatrix} = \gamma \begin{bmatrix} v_\alpha - v_{\mathrm{g},\alpha} \\ v_\beta - v_{\mathrm{g},\beta} \end{bmatrix}, \tag{5}$$

where $\gamma > 0$ is a positive scalar. The specific pre-synchronization sequence is as follows:

1) Keep the power reference $P^\star = 0$ and $Q^\star = 0$, while the grid switch S_1 is open and $(\mathrm{S}_2 \to \mathrm{b})$, the pre-synchronization controller is active and v_{abc} converges to $v_{\mathrm{g,abc}}$.
2) When the phase offset of v_{abc} with respect to $v_{\mathrm{g,abc}}$, denoted as δ, is smaller than some threshold ϵ, then S_1 is turned on and $(\mathrm{S}_2 \to \mathrm{a})$.
3) Change the power reference to achieve power delivery.

Below we analyze the behavior of the pre-synchronization controller discussed above, and show how it drives δ to zero in steady state.

B. Inverter Phase Angle and Frequency

With the oscillator input vector u in (5), the dynamics of voltage v_α and v_β are given as

$$\begin{bmatrix} \dot{v}_\alpha \\ \dot{v}_\beta \end{bmatrix} = \begin{bmatrix} \frac{\xi}{\kappa_{\mathrm{v}}^2}\left(2V_{\mathrm{nom}}^2 - \|v_{\alpha\beta}\|^2\right) & -\omega_{\mathrm{nom}} \\ \omega_{\mathrm{nom}} & \frac{\xi}{\kappa_{\mathrm{v}}^2}\left(2V_{\mathrm{nom}}^2 - \|v_{\alpha\beta}\|^2\right) \end{bmatrix} \begin{bmatrix} v_\alpha \\ v_\beta \end{bmatrix} - \frac{\kappa_{\mathrm{v}}}{C}\gamma \underbrace{\begin{bmatrix} v_\alpha - v_{\mathrm{g},\alpha} \\ v_\beta - v_{\mathrm{g},\beta} \end{bmatrix}}_{u}. \tag{6}$$

The inverter voltage phase angle θ is given by

$$\theta = \arctan\left(\frac{v_\beta}{v_\alpha}\right),$$

which induces the following dynamics corresponding to frequency

$$\dot{\theta} = \frac{v_\alpha \dot{v}_\beta - v_\beta \dot{v}_\alpha}{2V^2} = \omega_{\mathrm{nom}} + \frac{\kappa_{\mathrm{v}}\gamma}{C}\frac{v_\alpha v_{\mathrm{g},\beta} - v_\beta v_{\mathrm{g},\alpha}}{2V^2}, \tag{7}$$

where $V = \frac{1}{\sqrt{2}}(v_\alpha^2 + v_\beta^2)^{1/2}$ is the inverter voltage RMS value.

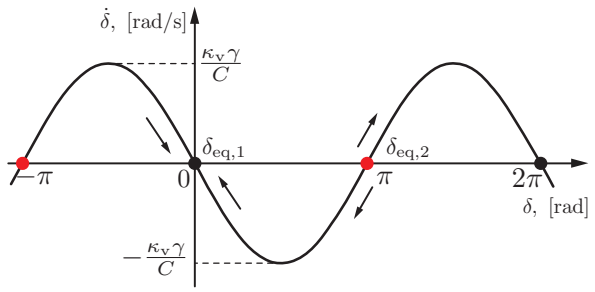

Fig. 2. Stable equilibrium points ($\delta_{\mathrm{eq},1} = 0, 2\pi, \cdots, 2k\pi$) and unstable equilibrium points ($\delta_{\mathrm{eq},1} = -\pi, \pi, \cdots, (2k-1)\pi$) for the phase-angle dynamics.

C. Kuramoto Model and Small-signal Stability

Using the trigonometric identities:

$$\cos\theta = \frac{v_\alpha}{\sqrt{2}V},\ \sin\theta = \frac{v_\beta}{\sqrt{2}V},$$
$$\cos\theta_{\mathrm{g}} = \frac{v_{\mathrm{g},\alpha}}{\sqrt{2}V_{\mathrm{g}}},\ \sin\theta_{\mathrm{g}} = \frac{v_{\mathrm{g},\beta}}{\sqrt{2}V_{\mathrm{g}}},$$

we can rewrite $\dot{\theta}$ as

$$\dot{\theta} = \omega_{\mathrm{nom}} + \frac{\kappa_{\mathrm{v}}\gamma}{C}\sin(\theta_{\mathrm{g}} - \theta), \tag{8}$$

with the assumption that $V_{\mathrm{g}} \approx V$ during the pre-synchronization process. Notice that (8) has the general form of the well-known Kuramoto model. The phase difference $\delta = \theta_{\mathrm{g}} - \theta$, with $\dot{\theta}_{\mathrm{g}} = \omega_{\mathrm{nom}}$, has the following dynamics:

$$\dot{\delta} = \omega_{\mathrm{nom}} - \dot{\theta} = -\frac{\kappa_{\mathrm{v}}\gamma}{C}\sin\delta. \tag{9}$$

Figure 2 plots the δ-$\dot{\delta}$ curve given by (9). In one single period $[0, 2\pi)$, there are two equilibrium points (by solving $\dot{\delta} = 0$): i) $\delta_{\mathrm{eq},1} = 0$ is a stable equilibrium point, whereas ii) $\delta_{\mathrm{eq},2} = \pi$ is an unstable equilibrium point. This is readily observable by defining $\Delta\delta := \delta - \delta_{\mathrm{eq}}$, where δ_{eq} is the equilibrium value. The dynamics of $\Delta\delta$ are obtained by suitably linearizing (9), and they are given by:

$$\Delta\dot{\delta} = -\frac{\kappa_{\mathrm{v}}\gamma}{C}\cos\delta_{\mathrm{eq}}\Delta\delta. \tag{10}$$

From above, we can validate that $\delta_{\mathrm{eq},1} = 0$ is a stable equilibrium point, while $\delta_{\mathrm{eq},2} = \pi$ is not.

IV. Equivalent Circuit Interpretation and Parameter Selection

To better explain the pre-synchronization process, in this section, we develop an equivalent circuit model. Moreover, we also outline how the parameter γ can be selected.

A. Equivalent Circuit Interpretation

Figure 3 depicts the equivalent circuit model corresponding to (8) and (9), in which the differential equations are interpreted as the voltage dynamics corresponding to the two capacitors C_1 and C_2. The phase angles θ_{g}, θ, and δ are represented by voltages in the circuit, while the frequency

$\omega_{\rm nom}$ is interpreted as a constant current source. For the capacitor C_1, the voltage dynamics $\dot{\theta}$ are given by

$$C_1\dot{\theta} = \omega_{\rm nom} + i, \tag{11}$$

which is equivalent to (8) with $C_1 = 1$ and

$$i = \frac{\kappa_{\rm v}\gamma}{C}\sin(\theta_{\rm g} - \theta).$$

The voltage across capacitor C_2 is δ; the ideal operational amplifier input polarities are supplied by a voltage source $\theta_{\rm g}$. The current flowing through C_2 is i, then the δ dynamics can be expressed as

$$C_2\dot{\delta} = i = \frac{\kappa_{\rm v}\gamma}{C}\sin(\theta_{\rm g} - \theta), \tag{12}$$

which is equivalent to (9) when C_2 is a negative unit capacitance. A negative capacitance indicates that the capacitor voltage δ will decrease with the current i. Figure 3 also illustrates the C_2 voltage $\delta(t)$, with θ_0 denoting the initial phase difference. The plot shows that δ decreases to zero after a certain time, denoted as $t_{\rm pre-sync}$, which will be quantified next.

B. Selection of Coefficient γ

The selection of γ is based on the converging speed. Define $t_{\rm pre-sync}$ as the period for δ to evolve from 0.9π to 0.1π phase difference. (We pick these limits without loss of generality.) By integrating (9) over this range of δ, we obtain

$$\begin{aligned} t_{\rm pre-sync} &= \int_0^{t_{\rm pre-sync}} {\rm d}t = -\frac{C}{\kappa_{\rm v}\gamma}\int_{0.9\pi}^{0.1\pi}\frac{1}{\sin\delta}{\rm d}\delta \\ &= -\frac{C}{\kappa_{\rm v}\gamma}\ln\tan\left(\frac{\delta}{2}\right)\Big|_{0.9\pi}^{0.1\pi} \approx \frac{3.68C}{\kappa_{\rm v}\gamma}. \end{aligned} \tag{13}$$

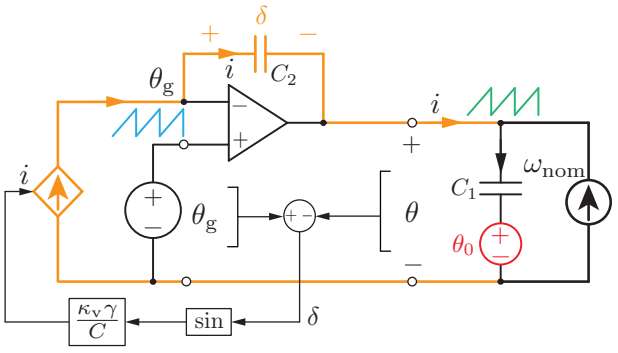

(a) equivalent circuit interpretation of the Kuramoto equation

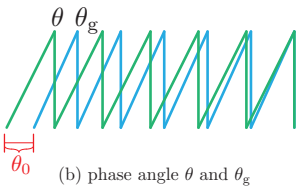

(b) phase angle θ and $\theta_{\rm g}$

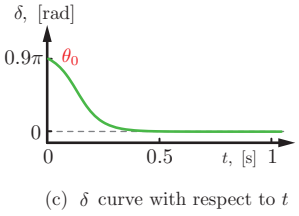

(c) δ curve with respect to t

Fig. 3. Equivalent circuit interpretation of pre-synchronization control strategy, (a) circuit model of Kuramoto model, (b) θ and $\theta_{\rm g}$, (c) δ.

TABLE I
NONLINEAR OSCILLATOR PARAMETERS.

Symbol	Description	Value	Units
$V_{\rm nom}$	Nominal oscillation amplitude	120	V
$\kappa_{\rm v}$	Voltage-scaling factor	120	V/V
$\kappa_{\rm i}$	Current-scaling factor	0.20	A/A
ξ	Speed constant	15	$1/{\rm sV}^2$
C	Virtual capacitance	0.2679	F
L	Virtual inductance	26.268	μH
γ	Scalar	0.025	–

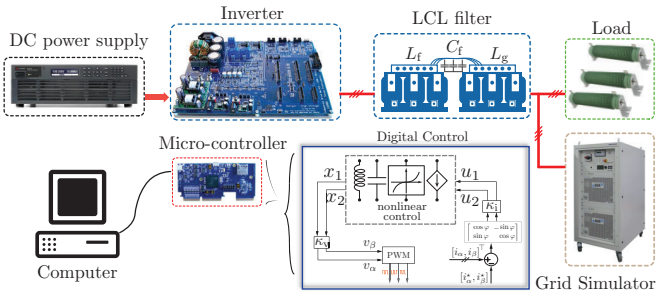

Fig. 4. A laboratory-scale experimental setup: A 1.5 kW LCL-filtered inverter controlled by a TI DSP.

The equation above shows that a larger γ will lead to a faster pre-synchronization process, whereas a smaller γ will contribute to a sluggish process. Hence, we can select a reasonable γ to satisfy the pre-synchronization time specification.

V. Experimental Validation

We built a laboratory-scale hardware prototype illustrated in Fig. 4 to validate the analytical developments. The filter components have the following values: inverter-side inductance $L_{\rm f} = 1.5$mH, grid-side inductance $L_{\rm g} = 1.5$mH, and filter capacitance $C_{\rm f} = 10\mu$F. The converter is a typical two-level H-bridge, with switching frequency set to $f_{\rm sw} = 10$ kHz. The nonlinear oscillator controls are programmed on a Texas Instruments TMS320F28379D micro-controller. The DC source is a regenerative DC supply at 320 V. Moreover, a grid emulator models a stiff grid at the inverter AC terminals.

An experiment is designed to demonstrate the pre-synchronization functionality to a stiff grid. Figure 6(a) shows waveforms corresponding to the pre-synchronization process: $v_{\rm g,ab}$ is the grid line-line voltage ($208{\rm V}_{\rm rms}$) and $v_{\rm ab}$ is the measured inverter voltage (we measure the filter capacitor $C_{\rm f}$ voltage instead, because we are not able to measure the inverter-terminal voltage directly). To evaluate feasibility for the worst-case scenario, the grid voltage $v_{\rm g,ab}$ is set to be $\delta \approx 180^\circ$ (which is inverse to the inverter voltage $v_{\rm ab}$) at the initial condition. Prior to the addition of pre-synchronization control (before time instant t_1), $v_{\rm ab}$ is inverse of grid voltage $v_{\rm g,ab}$; at t_1, the control is added, we observe that: $v_{\rm ab}$ actively regulates its frequency and angle θ to synchronize $v_{\rm g,ab}$ with some amplitude dip; after t_2, the phase difference $\delta \approx 0$ which

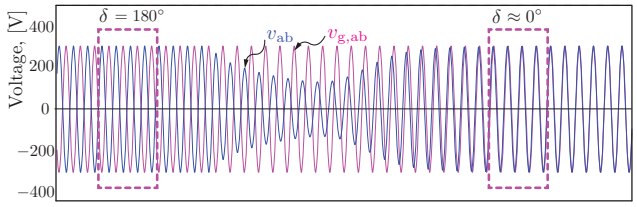

Fig. 5. Simulation results: pre-synchronization from 180° to 0° phase difference.

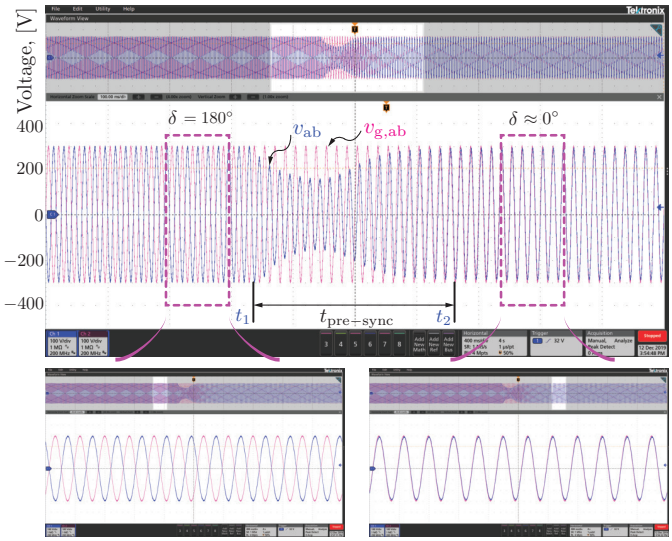

(a) phase difference: 180°to 0°

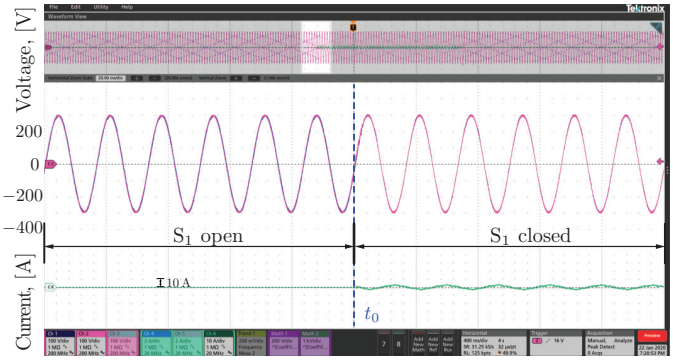

(b) switch S_1 acts at t_0

Fig. 6. Experimental results: pre-synchronization from 180° to 0° phase difference.

guarantee a safe and smooth grid connection process. In this paper, the scaling factor $\kappa_v = 120$ V, oscillator capacitance $C = 0.2679$ F [14]. In this experiment, we select $\gamma = 0.025$. (See Table I for a complete list of parameters, and [14] for the design process.)

According to (13), the calculated time $t_{pre-sync} \approx 0.4$s, which is in agreement to the results in Fig. 5 and Fig. 6 (a). Thereafter, Fig. 6(b) shows the transient current when switch S_1 closes at t_0. Before t_0, S_1 is open, current is zero; at t_0, there is almost no transient current which guarantee a smooth inverter addition; after t_0, some tiny reactive currents flow to filter capacitor.

VI. Conclusion

In this paper, we proposed a novel pre-synchronization method for virtual-oscillator controlled inverters to reduce startup transient inrush currents. An equivalent circuit model of the proposal is derived along with its dynamical properties, design guidelines are given, and experiments are shown. Experiment validation and analysis of adding inverters to a stiff grid using the proposed method are shown in this paper.

References

[1] L. A. Tôrres, J. P. Hespanha, and J. Moehlis, "Synchronization of Identical Oscillators Coupled Through a Symmetric Network With Dynamics: A Constructive Approach With Applications to Parallel Operation of Inverters," *IEEE Transactions on Automatic Control*, vol. 60, pp. 3226–3241, Dec. 2015.

[2] S. V. Dhople, B. B. Johnson, and A. O. Hamadeh, "Virtual oscillator control for voltage source inverters," in *2013 51st Annual Allerton Conference on Communication, Control, and Computing (Allerton)*, pp. 1359–1363, Oct. 2013.

[3] B. B. Johnson, S. V. Dhople, A. O. Hamadeh, and P. T. Krein, "Synchronization of Nonlinear Oscillators in an LTI Electrical Power Network," *IEEE Transactions on Circuits and Systems I: Regular Papers*, vol. 61, pp. 834–844, Mar. 2014.

[4] D. Raisz, T. T. Thai, and A. Monti, "Power control of virtual oscillator controlled inverters in grid-connected mode," *IEEE Transactions on Power Electronics*, vol. 34, pp. 5916–5926, Jun. 2019.

[5] M. A. Awal, H. Yu, H. Tu, S. M. Lukic, and I. Husain, "Hierarchical control for virtual oscillator based grid-connected and islanded microgrids," *IEEE Transactions on Power Electronics*, vol. 35, pp. 988–1001, Jan. 2020.

[6] J. Rocabert, A. Luna, F. Blaabjerg, and P. Rodríguez, "Control of power converters in AC microgrids," *IEEE Transactions on Power Electronics*, vol. 27, pp. 4734–4749, Nov. 2012.

[7] X. Wang, J. M. Guerrero, and Z. Chen, "Control of grid interactive AC microgrids," in *2010 IEEE International Symposium on Industrial Electronics*, pp. 2211–2216, Jul. 2010.

[8] M. Lu, S. Duan, C. Chen, J. Cai, and L. Sun, "Coordinate control of parallel connected power conditioning system for battery energy storage system in microgrid," in *2014 IEEE Applied Power Electronics Conference and Exposition - APEC 2014*, pp. 707–711, 2014.

[9] M. Ali, H. I. Nurdin, and J. Fletcher, "Dispatchable virtual oscillator control for single-phase islanded inverters: Analysis and experiments," *IEEE Transactions on Industrial Electronics*, 2020. Early Access.

[10] Z. Shi, J. Li, H. I. Nurdin, and J. E. Fletcher, "Comparison of virtual oscillator and droop controlled islanded three-phase microgrids," *IEEE Transactions on Energy Conversion*, vol. 34, pp. 1769–1780, Dec. 2019.

[11] D. F. Opila, K. Kintzley, S. C. Shabshab, and S. T. Phillips, "Virtual oscillator control of equivalent voltage-sourced and current-controlled power converters," *Energies*, vol. 12, pp. 298–315, Jan. 2019.

[12] B. Johnson, M. Sinha, N. Ainsworth, F. Dörfler, and S. Dhople, "Synthesizing Virtual Oscillators to Control Islanded Inverters," *IEEE Transactions on Power Electronics*, vol. 31, pp. 6002–6015, Aug. 2016.

[13] M. Sinha, F. Dörfler, B. B. Johnson, and S. V. Dhople, "Uncovering droop control laws embedded within the nonlinear dynamics of Van der Pol oscillators," *IEEE Transactions on Control of Network Systems*, vol. 4, pp. 347–358, Jun. 2017.

[14] M. Lu, S. Dutta, V. Purba, S. Dhople, and B. Johnson, "A grid-compatible virtual oscillator controller: Analysis and design," in *2019 IEEE Energy Conversion Congress and Exposition (ECCE)*, pp. 2643–2649, Sep. 2019.

[15] M. Colombino, D. Groß, J. Brouillon, and F. Dörfler, "Global phase and magnitude synchronization of coupled oscillators with application to the control of grid-forming power inverters," *IEEE Transactions on Automatic Control*, vol. 64, pp. 4496–4511, Nov. 2019.

[16] D. Groß, M. Colombino, J. Brouillon, and F. Dörfler, "The effect of transmission-line dynamics on grid-forming dispatchable virtual oscillator control," *IEEE Transactions on Control of Network Systems*, vol. 6, pp. 1148–1160, Sep. 2019.

[17] H. Yu, M. A. Awal, H. Tu, I. Husain, and S. Lukic, "Comparative transient stability assessment of droop and dispatchable virtual oscillator controlled grid-connected inverters," *IEEE Transactions on Power Electronics*, 2020. Early Access.
[18] B. B. Johnson, S. V. Dhople, A. O. Hamadeh, and P. T. Krein, "Synchronization of parallel single-phase inverters with virtual oscillator control," *IEEE Transactions on Power Electronics*, vol. 29, pp. 6124–6138, Nov. 2013.
[19] Z. Chen, W. Zhang, J. Cai, T. Cai, Z. Xu, and N. Yan, "A synchronization control method for micro-grid with droop control," in *2015 IEEE Energy Conversion Congress and Exposition (ECCE)*, pp. 519–524, 2015.
[20] W. Zhang, A. Luna, and P. Rodriguez, "Start-up of virtual synchronous machine: Methods and experimental comparison," in *2018 2nd IEEE Conference on Energy Internet and Energy System Integration (EI2)*, pp. 1–9, 2018.
[21] J. Jiao, R. Meng, Z. Guan, C. Ren, L. Wang, and B. Zhang, "Grid-connected control strategy for bidirectional AC-DC interlinking converter in AC-DC hybrid microgrid," in *2019 IEEE 10th International Symposium on Power Electronics for Distributed Generation Systems (PEDG)*, pp. 341–345, 2019.
[22] M. Awal and I. Husain, "Unified virtual oscillator control for grid-forming and grid-following converters," 2020. [Online] Available at: http://arxiv.org/abs/2007.06042.